Peptide Conformational Dynamics and Vibrational Stark Effects Following Photoinitiated Disulfide Cleavage

Martin Volk,[†,‡] Yuriy Kholodenko,[†] Helen S. M. Lu,[§] Edward A. Gooding,[†] William F. DeGrado,[§] and Robin M. Hochstrasser*[,†]

Department of Chemistry and Department of Biochemistry and Biophysics, The Johnson Foundation for Research in Biophysics, The University of Pennsylvania, Philadelphia, Pennsylvania 19104

Received: June 13, 1997; In Final Form: August 19, 1997[⊗]

Photoinitiation of relaxation of two peptides (labeled **1** and **2)** and spectroscopic studies of the ensuing dynamics have led to new information about peptide conformational dynamics. Following photolysis of the aryl disulfide chromophore that constrains a peptide to be distorted from its equilibrium form, the S−S bond is broken in <200 fs, and the liberated thiyl radicals either undergo geminate recombination or diffuse apart to allow the peptides to change conformation. From anisotropy measurements, overall peptide rotation is on the time scale of 600 ps. At an even earlier time (ca. 100 ps), transient IR measurements show a bleaching of the amide I′ region, arising from a vibrational Stark effect produced upon ring opening of peptide **2**. We did not detect any significant shift in the amide I′ region up to 2 ns, suggesting no significant helix formation in this time domain. Thiyl radicals arising from peptide **2** recombine with a power law rate over the time range from picoseconds to microseconds signaling an unusual type of scaled kinetics.

Introduction

This paper deals with optical triggering of peptide conformational dynamics. The triggering event is the dissociation of a disulfide bond to create two thiyl radicals, one at either end of a distorted helical peptide chain. A number of processes can be expected to occur after the light is absorbed. The bond-breaking step is known to occur on the femtosecond time scale from studies with model compounds.[1−3] After dissociation the radicals may undergo recombination to form the original disulfide. For model disulfides that are not constrained by the peptide the recombination has a geminate phase that is kinetically distinct from the diffusion-controlled bimolecular recombination. In the peptide a geminate phase is expected to develop into a diffusion-controlled recombination, controlled by the ability of the peptide to bring the radicals back to a reactive configuration. Thus an investigation of the time dependence of the radical populations provides information on the peptide conformational dynamics. If part of these conformational dynamics involves significant changes in the secondary structure of the peptide it could be exposed by means of transient infrared spectroscopy.[4,5] Finally there may be electronic influences on the peptide structure from the modified charges that appear after photodissociation, and again infrared spectroscopy can be used to detect any changes in vibrational frequency and cross section that result.

A number of papers have considered the kinetics of the encounters between the two ends of a polymer chain.[6−8] Even for idealized polymer structures such as in the Rouse model[9] this problem was not yet solved exactly, although the behavior is readily simulated for a given potential energy function. The disulfide peptides of the present work present the situation wherein the initial condition is a highly nonequilibrium distribution of diradical structures close to the reactive region. The final state is necessarily a fully recombined distribution of disulfide molecules even at infinite dilution of the peptide. The experiments we propose should provide fundamental information about the kinetics of such conformational changes while also laying the groundwork for subsequent studies of the dynamics of helix−coil transitions in protein folding and unfolding processes over a wide range of time scales.

The search for a detailed description of the dynamics that govern protein folding presents many challenging questions. Considerable progress already was made in the study of protein dynamics occurring from milliseconds onward.[10−12] However, protein folding dynamics range from picoseconds to seconds.[13] The side chain motions contribute on the picosecond time scale, and main chain conformational changes occur from nanoseconds to seconds. The motions of the secondary structures are likely to be instrumental in narrowing the configurational space of folding pathways and enabling proteins to fold efficiently. Therefore, it is of fundamental importance to study the ultrafast aspects of protein folding. Knowledge of the earliest steps of protein folding will also help to distinguish between the several mechanisms of protein folding such as the framework model,[10,14,15] the hydrophobic collapse model,[16−19] and the nucleation condensation model.[20−22] Furthermore, a deeper understanding of how proteins fold can guide in the design of proteins with novel functions.

There is both experimental and theoretical evidence for folding and unfolding on time scales much faster than a millisecond. Relaxation methods, such as dielectric relaxation[23] and ultrasonic attenuation,[24,25] show helix−coil relaxation times in the range of 10 ns to 10 μs. Large-scale structural changes were shown to occur on a time scale of 40 μs after the initiation of folding in cytochrome *c*.[26,27] A similar time constant was observed for the formation of a compact state during the folding of cold-denatured apomyoglobin after a *T*-jump.[28] Direct investigations were also performed with the help of fast laser-induced *T*-jumps. Unfolding features involving the solvation of β-sheets in RNase A after a *T*-jump were observed to occur in several steps on the few nanosecond-time scale.[4] Similarly, the unfolding of α-helices in apomyoglobin as well as the folding of α-helices in cold-denatured apomyoglobin after a

[†] Department of Chemistry. University of Pennsylvania.
[‡] Present address: Institut für Physikalische und Theoretische Chemie, TU München, Lichtenbergstr. 4, 85748 Garching, Germany.
[§] The Johnson Foundation for Research in Biophysics.
[⊗] Abstract published in *Advance ACS Abstracts,* October 1, 1997.

S1089-5647(97)01951-2 CCC: $14.00

SCHEME 1: Photoinitiation of α-Helix Formation

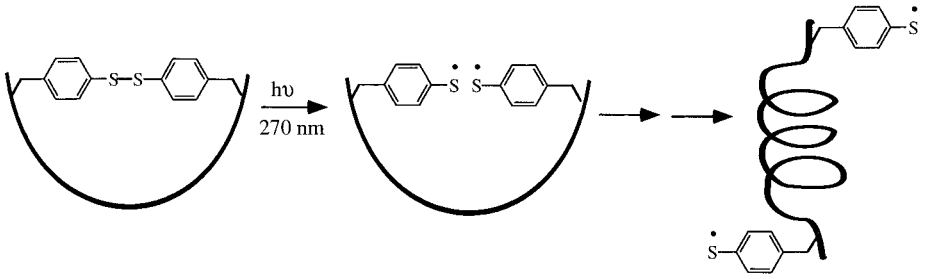

Peptide Sequence:

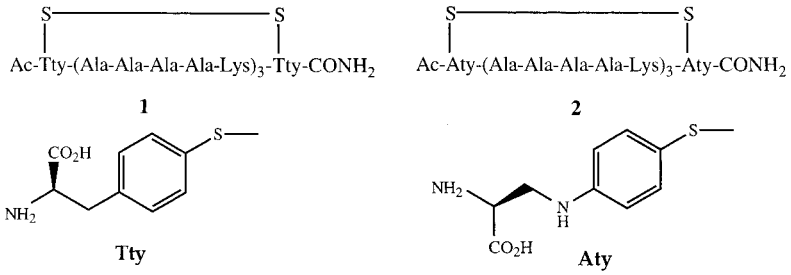

T-jump proceed on the time scale of 10−100 ns.[5] The unfolding of the suc-F_S 21-peptide, a short α-helical peptide that is similar to the peptides investigated here, proceeds with a time constant of 180 ns.[5,29] The transient IR absorbance changes in this peptide after a temperature jump also showed kinetics faster than the time resolution of the instrument (23 ns) and were attributed to a temperature-induced shift of the IR absorbance spectrum in the absence of helix unfolding and not to a fast unfolding component. However, it was not ruled out conclusively that they reflect the initial part of some nonexponential folding kinetics. Indeed, *T*-jump experiments on the same peptide labeled with a fluorescent probe at the N terminus exhibited a time constant of 20 ns for the relaxation of the first helix turn.[13] Theoretical studies of the folding of a short α-helix, using the Zimm−Bragg model for the equilibrium aspects of the helix to coil transition and explicit simulations of the thermodynamic barrier associated with helix initiation and propagation, estimated the folding/unfolding time scale in the 10 ns range.[30] Molecular dynamics simulations have predicted that α-helices can unfold on the sub-nanosecond time scale[31,32] and that ultrafast solvation of the hydrophobic regions[33] is an early stage of unfolding in barnase, in agreement with experimental results.[34] Some of the aforementioned investigations of protein folding dynamics which went beyond the millisecond time resolution of conventional rapid mixing techniques were recently reviewed.[13]

These experimental approaches all have their limitations: ultrasonic attenuation does not give direct structural information, *T*-jump experiments are limited to the induction of protein *un*folding, except for proteins that undergo cold denaturation, and ligand dissociation or electron-transfer triggering requires the presence of a cofactor. Our approach involves the laser-induced *initiation of a conformational change* of a polypeptide by *photochemical triggering*. The triggering process introduced here is photocleavage of an aryl disulfide cross-linking group which can be easily incorporated into polypeptides. The triggering mechanism is expected to be much faster than any expected conformational dynamics. To demonstrate the general utility of this approach, we report here the study of dynamics in a de novo designed peptide based on that reported by Baldwin.[35] This polyalanine peptide is known to be highly helical in solution. Circular dichroism (CD) studies indicate that the helicity of the cross-linked form is about half that of the unconstrained analogues, which have the same amino acid sequence, but no disulfide bond.[36] An illustration of a possible conformational change upon photolysis is depicted in Scheme 1, along with the sequences of the two peptides studied.

Experimental Details

Materials. The synthesis of peptides **1** and **2** as trifluoroacetate salts was previously described in ref 36. For measurements with visible probing light, the peptides were dissolved in H_2O, for IR measurements in D_2O. A temperature-stabilized flow-cell with CaF_2 windows and an adjustable path length was used. The path length was adjusted to 1 mm for measurements in the visible and to 50 μm for IR measurements. The concentration of the samples was adjusted to yield an absorbance of 1 ± 0.2 at 270 nm for the respective path length. The sample was flowed to ensure the rapid exchange of the excited volume. If not stated otherwise, the results presented below refer to a sample temperature of 31 ± 2 °C.

The stability of the peptides was checked by comparing ground-state absorbance spectra taken before and after the measurements and by high-performance liquid chromatography (HPLC) on the samples after the measurements. No indications of sample degradation during the measurements were found.

Methods. The femtosecond spectrometer used here was based on a home-built Ti:sapphire−oscillator/amplifier system, consisting of an Ar^+-laser pumped self-mode-locked oscillator,[37] a YLF laser-pumped regenerative amplifier, and a stretcher/compressor.[38] It yielded pulses at 810 nm with a duration of 75 fs and an energy of 300 μJ at a repetition rate of 1 kHz. Approximately 70% of the amplified light was split off and frequency-doubled and -tripled with two BBO crystals. Pulses with an energy of 4 μJ and a duration of 140 fs were obtained for disulfide photolysis at 270 nm. For some measurements, these pulses were further stretched to 500 fs by passing them through four prisms. This procedure reduced the intensity while maintaining the pulse energy, so that the production of solvated electrons by two-photon absorbance of water at 270 nm was minimized. The pump intensity was adjusted to avoid saturation of the sample: typically 0.5−1 μJ pump energy was focused on a spot with a 200 μm diameter for measurements with the

pump and probe beam polarizations at the magic angle (54.7°). For the measurements with IR probing light, pump energies around 2 μJ were used in order to improve the signal-to-noise ratio.

Visible probe light was obtained from a continuum, generated by focusing the 810 nm pulse into water. Selection of probe wavelengths (460−690 nm) was accomplished by 10 nm bandpass interference filters. IR probing light around 6 μm was generated in an optical parametric amplifier using a 2 mm $AgGaS_2$ crystal[39] with the continuum as seed light. The IR light thus generated had a spectral width of typically 150 cm^{-1}. A spectral resolution of 15 cm^{-1} was obtained in the IR by using a 22 cm focal length monochromator with a 150 lines/mm grating (blazed for 6 μm) before the sample.

The probe pulses were delayed with respect to the pump pulses by means of an optical delay line with a maximum delay of 3.5 ns and focused on the sample. The pump and probe beam directions made an angle of 5° at the sample. Time zero was determined with an accuracy of ±20 fs by means of pump/probe experiments on model systems. These experiments also allowed an estimate of pump−probe cross-correlation widths, yielding 220−280 fs and about 400 fs for the visible and IR probes, respectively, measured without stretching the pump pulse. Probing light in the visible/near IR and in the 6 μm region was detected with Si diodes and with liquid-nitrogen-cooled HgCdTe detectors, respectively; the signals were sent to a boxcar amplifier and digitized with fast A/D converters. A chopper reduced the excitation rate to 500 Hz, allowing the simultaneous measurement of the absorbance with and without excitation.

Normally, the polarization of the probe light was adjusted to be at the magic angle with respect to the polarization of the pump light. For anisotropy measurements, the angle between pump and probe polarizations was adjusted to 45°. The probe beam was split with a polarizer after the sample, and the two polarized absorption components $\Delta A_{||}$ and $\Delta A_{\perp}$ were detected separately. In this way transient absorption signals for parallel and perpendicular polarization of pump and probe light could be observed simultaneously at each delay time, allowing the calculation of the *anisotropy*:

$$r(t) = \frac{\Delta A_{||} - \Delta A_{\perp}}{\Delta A_{||} + 2\Delta A_{\perp}} \quad (1)$$

The anisotropy can be related to correlation functions of the transition dipoles involved in the pumping and probing processes (see Discussion). The experimental values of the anisotropy are useful for determining the orientational dynamics if the fraction of molecules in the sample that are photodissociated is kept less than ca. 10%.[40] Less than 0.5 μJ pump energy, focused to a spot size of 200 μm, was used for the anisotropy measurements. The fractional conversions obtained with these conditions were 3% for peptide **1** ($\epsilon_{270} = 4000\ M^{-1}\ cm^{-1}$) and 10% for peptide **2** ($\epsilon_{270} = 12\,000\ M^{-1}\ cm^{-1}$). The average degree of saturation was estimated in each experiment by averaging the pump intensity over the path length, assuming an exponential decrease in the sample.

For measurements on the nanosecond-time scale, the sample was excited by the fourth harmonic (266 nm) of a Q-switched Nd:YAG (DCR-1A, Quanta Ray, pulse duration 8 ns). The pump energy of 1.7 mJ was focused on a 10 × 2 mm^2 spot with a cylindrical lens. Probe light from a Xe lamp was split in two beams, yielding measuring and reference light, both of which traversed the sample normal to the actinic beam on a 1 cm path. The two beams were collected separately, dispersed in a monochromator, and detected in an intensified dual diode array system with a gate duration of 5 ns. The timing between pump laser pulse and gate was controlled electronically. More details of this apparatus are given in ref 41.

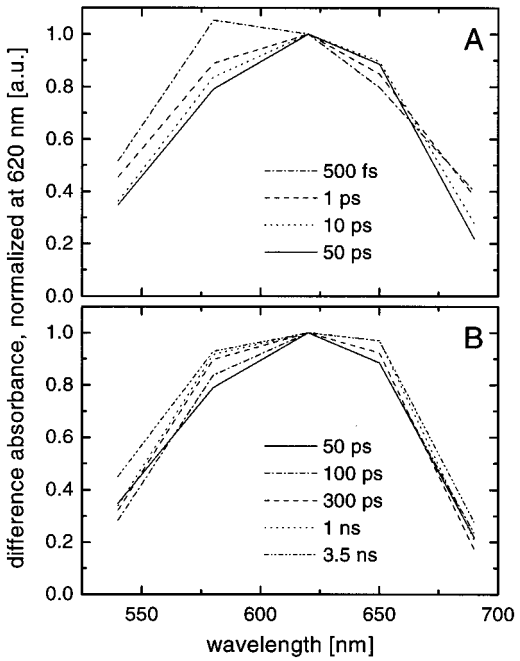

Figure 1. Transient spectra observed at the indicated delay times after excitation of peptide **2** at 270 nm, normalized to 1 at 620 nm.

Corrections for the Solvated Electron Signal. Intense femtosecond UV pulses lead to the ionization and dissociation of water via a two-photon process.[42] The resulting solvated electron has a strong absorption in the visible spectrum that overlaps the absorption of the thiyl radicals and interferes with the measurements. The localization, relaxation, and solvation of the electron created in this process have been investigated in great detail.[43−47] Within 500 fs after photoionization, the electron reaches its solvated ground state, which has a broad featureless absorbance in the visible/NIR spectral region with a maximum near 700 nm. Significant geminate recombination of the solvated electron and the cation is observed on the 10−100 ps time scale.

To check for possible distortions of the observed transient absorbance signals by solvated electrons, we performed measurements on water and on peptide samples under identical conditions. Significant solvated electron signals with spectral and dynamic characteristics as reported in the literature were observed (see inset of Figure 2). The solvated electron signal depended quadratically on the pump intensity at 270 nm, as expected from a two-photon process. With pump pulses of 140 fs, the solvated electron absorbance observed in neat water typically amounted to about 10−30% of the maximum transient absorbance observed in the peptide samples. By stretching the pump pulses to 500 fs while maintaining the same pulse energy, the expected reduction of the solvated electron signal by a factor of about 3 was achieved. All transient absorbance data in the visible spectral region shown below were obtained with stretched pump pulses unless otherwise indicated. No signals from solvated electrons in neat water were observed when probing in the IR region between 1600 and 1700 cm^{-1}; therefore unstretched pump pulses were used in these experiments. No solvated electron signal was obtained with neat water pumped with the nanosecond pulses at 266 nm.

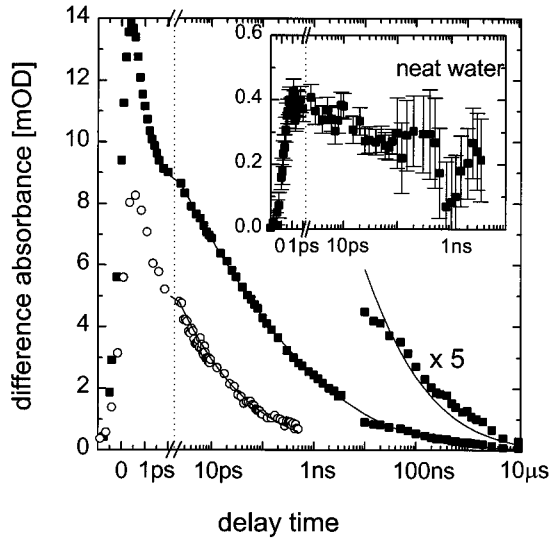

Figure 2. Decay of the thiyl radical absorbance in peptide **1** (○, 500 nm) and peptide **2** (■, 620 nm) after excitation at 270 nm. Error bars, given by the standard deviation of the measurement, are smaller than the size of the symbols. Solid lines are best fits of the data after 2 ps to a stretched exponential function, as described in the text (results: peptide **1** $\alpha = 0.07-0.10$, $\langle\tau\rangle = 150$ ps; peptide **2** $\alpha = 0.09-0.10$, $\langle\tau\rangle \approx 100-500$ ns). Note that the time scale is linear below 0.002 ns and logarithmic above 0.002 ns. Inset: Solvated electron signal, measured at 620 nm on neat H_2O under identical conditions.

A measurement on neat water was taken under identical conditions after each peptide experiment, and the two results were subtracted after making an adjustment for the decrease of the squared pump intensity along the optical paths, which is different in the water and the peptide samples. All data in the visible spectral region obtained with femtosecond pump pulses were corrected for the solvated electron signal in this way.

Deposition of Heat by the Laser Pulse Excitation. In the optical triggering experiment it is not possible to avoid heating the sample as a result of the absorption of light from the 270 nm pump beam. Any nonradiative processes such as internal conversion, intersystem crossing, and the chemical reaction itself will deposit some fraction of the energy of the absorbed photon into the solvent as heat. The ensuing temperature rise will depend on the number of absorbed photons, the efficiency of the nonradiative process, and the heat capacity of the solvent. While the effect of this rise in temperature on optical spectra is often negligible, it cannot be ignored in infrared pump−probe experiments carried out in water. The IR spectrum of water (and D_2O) is extremely temperature sensitive,[4,48] and the probe pulse is absorbed significantly by the water in both the pumped and unpumped samples. For the conditions of our experiment a maximum temperature increase in the excited volume of 0.5 °C can be estimated. This assumes that all of the pump energy is being deposited in the solvent as heat, and it leads to a D_2O absorbance change of less than 0.5 mOD at 1630 cm^{-1}.[4] However, the disulfide bond dissociation yield of 10% at 0.5 ps, estimated from our measurements described below, indicates that there can be other loss channels from the excited state of the aryl disulfides. If these other channels were to populate electronically excited states having lifetimes in excess of 2 ns, only a fraction of the pump energy would contribute to D_2O heating on this time scale, and an even smaller solvent signal would be expected. To circumvent the uncertainty in the fraction of the energy leading to solvent heating on the time scale of the measurement, we used the known shape of the IR difference spectrum caused by heating D_2O,[4] along with the transient IR measurements on the peptide samples in spectral regions removed as far as possible from the amide I′ peak, to determine the corrections needed at the amide I′ peak.

Results

A number of different types of measurements were carried out. The magic angle transient absorption in the visible measures the time dependence of the *population of thiyl radicals* generated following dissociation of the −S−S− bond by the 270 nm pump pulse. The measurement of the survival probability of these radicals is the major part of this work. The anisotropy of this signal provides key information regarding the time dependence of *the orientational distribution* of these radical absorbers. The infrared transients probe directly the amide I′ spectral region and measure its responses to the disulfide bond splitting. The amide I′ spectrum is sensitive to changes in the structure around the peptide carbonyls and to electric fields at these carbonyls introduced by the triggering process.

Transient Absorbance in the Visible. Photolysis of peptides **1** and **2** at 270 nm led to transient absorbances peaking at 500 and 620 nm (see Figure 1), respectively. These transients appeared within the ca. 100 fs time resolution of the instrument. The transients compare well with typical absorbance spectra of *p*-aminophenylthiyl radicals and *p*-tolylthiyl radicals,[1,49,50] showing that fast photocleavage of the disulfide bond has taken place. From the observed transient absorbance[51] we estimated a disulfide bond dissociation quantum yield of 0.10 ± 0.04 *at a delay time of 0.5 ps* for peptide **2**. A more accurate determination of the quantum yield is difficult because the extrapolation of the radical absorbance to zero time is highly uncertain as a result of the nonexponential initial kinetics.

The transient spectrum of the aminophenylthiyl radical exhibits a time dependence (Figure 1). In the first few picoseconds the peak of the band shifts from 580 to 620 nm (Figure 1A), accompanied by a sharpening of the low-energy edge of the spectrum. This behavior is similar to that observed for *p*-aminophenylthiyl radicals after photolysis of bis(*p*-aminophenyl) disulfide in acetonitrile,[2] which was attributed to dielectric and vibrational relaxation. Part of the shift is believed to arise from an internal charge separation between the amino group and the sulfur atom,[1] as is discussed further below. On a longer time scale, the width of the absorbance band (fwhm) increases from 115 nm at 50 ps to 130 nm at 3.5 ns without any significant shift of the position of the maximum (Figure 1B). This broadening probably is a result of internal peptide motions. These motions are expected to lead to a more inhomogeneous distribution of radical environments and thus to spectral broadening (see below).

The phenylthiyl and *p*-aminothiyl radicals generated from peptides **1** and **2** showed notable differences in their decay kinetics, evident in Figure 2. Both peptides show an initial rapid decrease in absorbance in the first few picoseconds. In peptide **1** the absorbance continues to decay and the signal is essentially gone by 800 ps. In contrast, for peptide **2** the absorbance changes were still observable up to 10 μs. The rapid initial decay from both peptides is attributed to geminate recombination of the pairs of radicals created by the photolysis pulse. This interpretation is consistent with studies of model compounds. Significant geminate (cage) recombination of phenylthiyl radical pairs was seen after photolysis of diphenyl disulfide.[1,52] On the other hand, no geminate recombination of aminophenylthiyl radical pairs was detected after photolysis of bis(*p*-aminophenyl) disulfide in polar solvents.[1] We designed peptide **2** based on this reported lack of geminate recombination of *p*-aminothiyl radicals. The inefficient recombination of aminophenylthiyl radicals in polar solvents was attributed[1] to strong solvation of

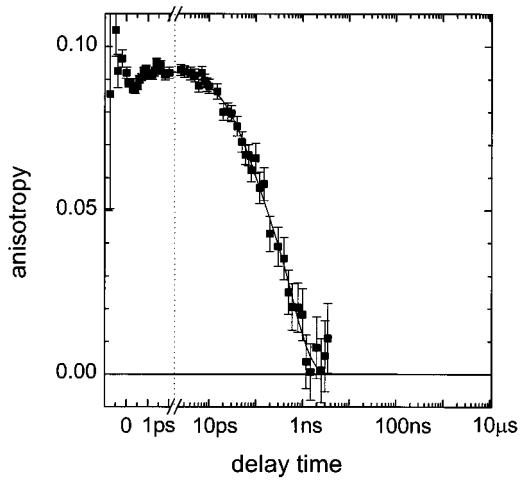

Figure 3. Anisotropy decay of the aminothiyl radical absorbance at 620 nm in peptide **2** at 31 °C. The solid line is the best fit to a biexponential decay, yielding time constants of 60 ps (relative amplitude 30%) and 600 ps (70%).

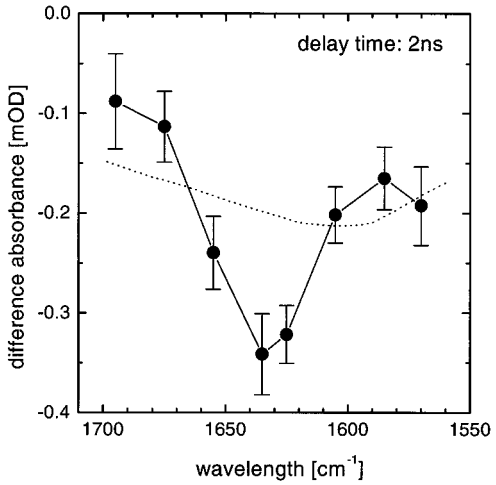

Figure 4. Difference spectrum in the amide I′ region of peptide **2** in D_2O at 10 °C at a delay time of 2 ns after excitation. The dotted line represents the spectral shape of the signal due to heating of D_2O (scaled to the signals dominated by D_2O farthest from the amide I′ peak).

the separated radicals. The radicals become polar as a result of an internal charge transfer between the amino group and the sulfur atom.[49] The formation of this solvent-stabilized charge-separated state occurs on the picosecond time scale, as indicated by shifts of the transient aminophenylthiyl radical absorbance spectrum in polar solvents.[1] Our results suggest that the solvation of the polar aminophenylthiyl radicals of peptide **2** is also completed on the time scale of a few picoseconds.

The recombination kinetics of peptides **1** and **2** proceed with nonexponential kinetics, over 7 orders of magnitude in time for peptide **2**. The radical recombination kinetics for both peptides is quantitatively described by a stretched exponential absorbance, $y = A_0 \exp(-(k_0 t)^{\alpha})$. A value of 0.1 ± 0.01 for the exponent, α, was found for both peptides, implying that in each case the same underlying process is responsible for the kinetics of thiyl radical recombination. The "average lifetimes," given by $(\alpha k_0)^{-1}\Gamma(\alpha^{-1})$, are approximately 150 ps for peptide **1** and 100−500 ns for **2.** To assess the temperature dependence of the recombination, peptide **2** kinetics was measured between 0 and 3 ns at 12 and 31 °C. Similar results were obtained at the two temperatures.

The Anisotropy. The anisotropy of the transient absorbance of the radical from peptide **2** is shown in Figure 3. At 12 °C a satisfactory fit to a monoexponential decay yielded a time constant of 500 ps; a biexponential fit yielded 40 ps (with a relative amplitude of 12%) and 610 ps (88%). At 31 °C, where a better signal-to-noise ratio was achieved, no satisfactory fit to a monoexponential could be obtained. A fit to a biexponential yielded time constants of 60 ps (30%) and 600 ps (70%). The total anisotropy from the biexponential fit extrapolated to zero time was 0.093 ± 0.01.

Transient Infrared Absorbance in the Amide I′ Region. The amide I′ band[53] of peptides and proteins, which mainly involves the carbonyl stretching vibration of the peptide backbone, is a sensitive marker of peptide secondary structure.[54] The vibrational frequency of a particular C═O bond depends on hydrogen bonding and the interactions between the amide units, both of which are influenced by the secondary structure. The IR spectrum of peptide **2** in the amide I′ region at room temperature, corrected for the D_2O background absorbance, shows two maxima: one at 1672 cm^{-1} is assigned to the carboxylate of the trifluoroacetate counterion, and another at approximately 1640 cm^{-1} is assigned to the amide I′ band of the partially unfolded peptide, which contains α-helical as well as coil structural elements.[36] This interpretation is in good agreement with the structural calculations and the CD results,[36] both of which evidence partial α-helix formation in the constrained peptide **2**. After splitting of the disulfide bond, the helical content of the peptide is expected to increase to the amount found in the unconstrained peptide. Accordingly, the amide I′ band should shift if, after disulfide bond cleavage, the helical structure begins to form. Significant progress toward α-helix formation implies that the thiyl radicals escaped from the initial clasping peptide conformation, thereby extending the lifetime of the radicals. Since peptide **1** exhibits close to 100% geminate recombination on the subnanosecond time scale, only a small fraction of the molecules will manage to escape the clasp and fold into the nonconstrained form. Therefore we carried out the time-resolved IR measurements only on peptide **2**, which, with its long thiyl radical lifetime, is more likely to have significant population that escapes the recombination. The time-resolved difference IR spectrum in the amide I′ region of peptide **2** in D_2O at 12 °C, measured at a delay time of 2 ns after disulfide bond splitting, is shown in Figure 4. Also shown is the shape of the expected spectral changes from the heating of D_2O, as determined from FTIR spectra of D_2O at different temperatures (see the Methods subsection). The resulting infrared difference spectrum of peptide **2** shows a clear bleaching and/or broadening of the amide I′ band at 1640 cm^{-1}. There is no observable shift of the amide I′ band from 100 ps to 2 ns.

The time dependence of the transient absorbance at 1605 and 1630 cm^{-1} at delay times beyond 100 ps is shown in Figure 5A.[55] As discussed in the Methods subsection the signal at 1605 cm^{-1} is dominated by the heating of D_2O, whereas the peptide dominates the signal at 1630 cm^{-1}. Figure 5B shows the resulting peptide **2** absorbance obtained after subtraction of the heating contribution. It corresponds to a bleach of the amide I′ band that appears rapidly compared with 100 ps and then decays in parallel with the disappearance of the thiyl radical absorbance, which is also shown in the figure. This result suggests that the thiyl radical population kinetics and the IR bleaching recovery are responses to the same physical process.

Discussion

This paper describes the first example of the use of disulfides as photodissociable cross-linking groups to initiate peptide dynamics. Disulfides appear to be ideal for this application, as they provide both a dissociable bond and an intrinsic probe of conformational dynamics through the survival probability of the

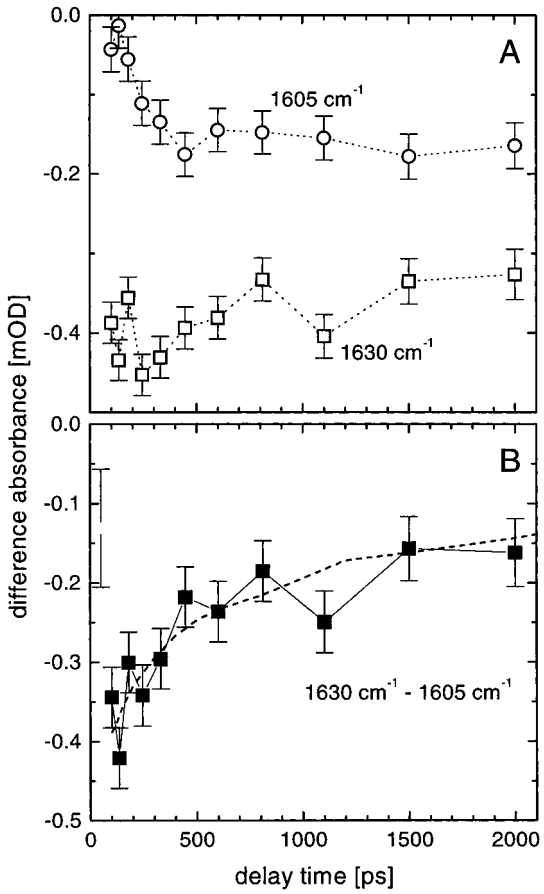

Figure 5. (A) Time dependence of the transient absorbance of peptide **2** in D_2O at 10 °C at 1630 cm^{-1} (□) and 1605 cm^{-1} (○) for delay times above 100 ps. (B) Difference between the measurements at the two wavelengths (■). The dashed curve represents the decay of the aminothiyl transient absorbance at 620 nm at delay times above 100 ps, inverted and scaled to the difference curve.

radicals. The time frame for the conformational processes that can be probed with thiotyrosine derivatives is determined by the rates of phototriggering and recombination. The rate of photodissociation of the −S−S− bond is extremely fast and occurs in the sub-picosecond time frame, and the rate of recombination can be fine-tuned through the incorporation of appropriate substituents onto the thiophenyl ring. In the present application, two derivatives were examined. While thiotyrosine was found to recombine too quickly to be useful for studying processes involving backbone dynamics, the incorporation of a *p*-aminoalkyl group increased the lifetime sufficiently to allow investigation of changes in the radical populations occurring on the picosecond to microsecond time scale.

The cleavage of the aminothiotyrosine disulfide bond generates a species whose backbone conformation can be directly probed by time-resolved visible and IR spectroscopy. The visible absorption spectrum of the radical intermediate has a high extinction coefficient (approximately 20 000 M^{-1} cm^{-1}); it can be observed out to the microsecond time scale, providing information concerning conformational dynamics through observation of the peptide ends. In the peptide, approximately 90% of the initially generated material had recombined within about 2−5 ns. This time scale provides an upper limit for direct measurement of the helix by IR given our experimental setup, the quantum yield for disulfide cleavage, and the change in extinction coefficient for the amide I′ band. Recent time-resolved studies of helix formation have shown that the IR signature of helixes appears with time constants ranging from 20 to 200 ns, so we do not expect to directly observe the early

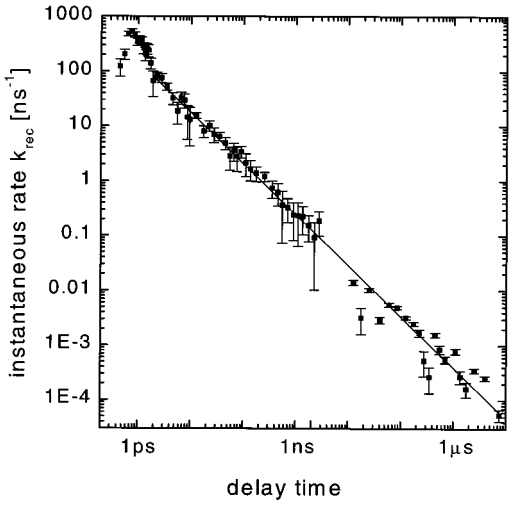

Figure 6. Instantaneous rate constant $k_{rec} = -y^{-1}(dy/dt)$ for the decay of the transient thiyl radical absorbance y at 620 nm in peptide **2** at 31 °C. The solid line is a linear fit of the logarithm of the instantaneous rate vs the logarithm of the delay time for delay times above 2 ps, yielding a slope of -0.93 ± 0.02.

stages of helix formation by transient IR spectroscopy. However, we do expect to observe the electronic effects on the carbonyls as a result of disulfide bond cleavage. The aminothiyl radical has a significant dipole moment, not present in the aminothiotyrosine disulfide, so that on photocleavage the nearby amide groups suddenly experience an additional electric field. This field can cause changes in the peptide IR spectrum.

Peptide Control of the Radical Recombination Dynamics. The photodissociation of the disulfide bond generates two free thiyl radicals caged by the solvent and clasped by the constraints provided by the peptide to which they are attached. The model aminophenylthiyl radical compound in solution does not exhibit significant geminate recombination. The radicals simply escape from the cage and recombine through diffusion-controlled kinetics that depend on the initial concentration of disulfides. On the contrary, extensive geminate recombination occurs in peptide **2**, which contains the same aminothiotyrosine disulfide unit. This result strongly suggests that the recombination kinetics in peptide **2** is determined by peptide structural effects. Therefore the detailed study of the thiyl radical population as a function of time is expected to yield novel information regarding the peptide dynamics.

The transient thiyl radical absorbance $y(t)$ can be used to calculate the instantaneous rate constant $k_{rec} = -(dy/dt)/y$ for radical recombination. Figure 6 shows this instantaneous rate constant for peptide **2** at 31 °C. For delay times longer than 2 ps, after the initial spectral shifts are largely completed, the logarithm of the instantaneous rate constant depends linearly on the logarithm of the delay time. A fit yields a slope of -0.93 ± 0.02. Thus, the instantaneous rate constant follows a power law in time: $k_{rec} \propto t^{-0.93}$. This power law holds over the entire 7 orders of magnitude in time examined. A power law behavior also was observed for radical recombination in peptide **1**, with the linear fit yielding a slope of -0.97 ± 0.09. Due to the faster radical recombination in peptide **1**, only 3 orders of magnitude in time (from 2 ps to 2 ns) could be examined experimentally.

This power law behavior of the recombination rate constant with an exponent near −1, observed over 7 orders of magnitude in time in peptide **2**, is quite remarkable. By comparison, if the rate of radical recombination followed a simple first-order rate law, the instantaneous rate constant would be invariant with time. A diffusion-controlled, bimolecular second-order process

involving the recombination of radicals from different peptides would yield a recombination rate constant inversely proportional to the time at sufficiently long times. However, a simple estimate shows that this process is much too slow to significantly contribute to the observed rate, given the low concentration of radicals, ca. 10^{-5} M, and assuming a bimolecular rate constant of 10^9 M^{-1} s^{-1}.

The observed $1/t$ behavior of the rate constant of recombination is in contrast to the expectations from simple diffusion models. Assuming free diffusion of the peptide ends, one would expect the probability of collisions to decrease as $t^{-1.5}$. The introduction of a potential (e.g. a harmonic spring model) does not affect the initial free diffusion behavior. Deviations from the $t^{-1.5}$ behavior are expected only after diffusion has taken place over the length scale of the potential. On this time scale the collision probability and the recombination rate constant will assume a constant value, with the transition from $t^{-1.5}$ to constant occurring in less than two decades of time. Thus, other explanations of the wide range of t^{-1} behavior have to be sought.

The population of the diradical state generated by the excitation pulse exhibits a monotonic decrease with time and tends to zero as time goes to infinity. This implies that the spectra of the radicals at the ends of the peptide are insensitive to any nonmonotonic changes that might be occurring in the secondary structure of the peptide, such as a coil to helix transition. More importantly, our results indicate that throughout the whole period of existence of a diradical population the structure fluctuations are large enough to ensure that ultimately there will be complete recombination of the radicals. If the helix does form on the nanosecond time scale, its structural fluctuations would have to be adequate for recombination of the ends to occur on the micro- to millisecond time scale. Additionally, the effectiveness of these fluctuations in bringing about radical recombination must scale monotonically over the whole observation time period.

Another scenario to consider is that the photolysis of the inhomogeneous sample generates a broad distribution of diradical structures, *none* of which ever reach the stable helix form. Then the survival probability would be determined simply by the corresponding radical pair spatial distribution, with each structure undergoing recombination according to its own diffusional or barrier-crossing dynamics. Although this was not excluded by direct test, it seems unusual that a range of time scales for recombination as wide as was observed could arise if the initial condition is a distribution of relatively *short* interradical distances. Moreover it seems improbable that less than 10^{-7} of the nascent structures would manage to escape and evolve toward more helical forms in the time available.

The universality of the power law behavior over the full experimental time scale would argue for a single underlying phenomenon, which we propose to be associated with conformational relaxation of the peptide. Qualitatively, the decrease in the observed rate can be understood in terms of a series of conformational changes that, as time progresses, increase the inter-radical distance *and* change the time scales of the peptide motions. After cleavage of the disulfide bond, the sulfur atoms are initially very close, and the peptide structure allows them to recombine rapidly. However, as time progresses, the fraction of less reactive states with longer inter-radical distances increases *and* the peptide might become less flexible (as its helical content increases), accounting for the decreasing rate. Such a picture can lead to fractal-like kinetics where there is self-similarity between processes occurring in each of the time regimes, and power law behavior can be expected.[56]

A number of different conformational processes, each with different time scales bracketing the experimental time scale of interest, are known to exist for the aminotyrosine-containing peptide. Side chain reorientation associated with changes in the $\chi_1$and χ_2 angles of the aminotyrosine residue should be expected to contribute on the picosecond time scale. It is possible that the faster correlation time associated with the radical absorbance anisotropy decay is influenced by such side chain reorientations. Main chain conformational changes associated with helix formation may begin to occur on the nanosecond time scale. In particular, the kinetics of partial melting and reformation of monomeric α-helices has recently been investigated in IR or fluorescence monitored *T*-jump experiments. These studies showed that the rate constant for extension of a preinitiated helix is on the order of 10^7-10^8 s^{-1}.[29] In addition, because the cyclic peptide begins in a largely nonhelical conformation, many of the chains may not have a preinitiated helix at the time of the photolysis. As a result, helix formation in these chains would probably occur on a longer time scale, because helix initiation is approximately 1000-fold less favorable than helix elongation.[25,57] Thus, well-established conformational processes should be expected to occur from the picosecond out to the microsecond range. A detailed understanding of how these processes contribute to the observed time dependence of the rate of recombination of radicals connected to the ends is a theoretical challenge.

The Orientational Diffusion of the Peptide Ends. The anisotropy of the thiyl radical absorbance in peptide **2** provides information about the rotational diffusion of the modified tyrosines at the peptide ends. The observed $r(t)$ is determined by the ensemble average of the second Legendre polynomial, $P_2(\cos\theta)$, of the cosine of the angle, θ, between the transition dipoles for the pumped and probed states. In the present case a disulfide absorption band is pumped for which the transition dipole moments are combinations of those from the two tyrosines. The probed transition of the radical is uniquely polarized along the −C−S bond axis. The observed peak anisotropy of 0.093 is determined by some unknown properties. The excitation leading to photodissociation may involve more than one electronic transition of the undissociated peptide. The anisotropy is also reduced because the probed radical may or may not be the one attached to the absorbing tyrosine.[58] However, it is the rotational diffusion of the transition dipole vector along the −C−S bond that causes the reduction in anisotropy as time progresses. The overall anisotropy with contributions from ends 1 and 2 of the diradical can be written as

$$r(t) = A\langle P_2(\cos\phi_1[t])\rangle + B\langle P_2(\cos\phi_2[t])\rangle \qquad (2)$$

where $\phi[t]$ is the angle between the −C−S bond at one of the ends at times 0 and t. The limiting anisotropy $r(0)$ is $A + B = 0.093$. The constants A and B depend on the details of the various pumped transitions,[59] and $\langle ... \rangle$ represents an ensemble average.

The anisotropy of peptide **2** was observed to decay on the hundreds of picosecond time scale: a biexponential fit yielded time constants of 60 ps (30%) and 600 ps (70%) at 31 °C. The overall rotational dynamics of the de novo peptides investigated here can be estimated by applying the Perrin model,[60] which assumes stick boundary conditions. The structural calculations, described in more detail elsewhere,[36] show that the instantaneous shapes of the constrained peptides can be approximated by ellipsoids with axis lengths in the range 9−20 Å. Rotational diffusion times were determined for a representative set of these calculated structures. The values were found to be in the range 400−650 ps which should be compared with the experimentally

observed time constant of 600 ps. These calculations were treated as estimates of the rotational correlation times and used only to confirm that overall motion is expected on the observed time scales. The comparison supports the attribution of the slower component of the anisotropy decay to the rotational diffusion of the whole peptide signaled by the anisotropic absorption of the radicals at the ends. However, the 60 ps component must be attributed to rotational diffusion of the tyrosine ends relative to the whole protein. The motion of the tyrosine ends seen through the 60 ps compononent of the anisotropy corresponds to a reduction of the order parameter to 0.7: If the −C−S direction were confined to diffuse within a cone,[61] the cone angle would be 38°. Our results, which show just two exponential time constants, indicate that both ends of the peptide have the same diffusional dynamics within experimental error; that is, the two time dependent terms in eq 2 are equal at all times. These results also indicate that no significant peptide backbone motions that modify the orientations of the −C−S bonds occur before a few hundred picoseconds: such motions would speed up the loss of anisotropy.

IR Transients in the Amide I′ Region. As discussed earlier, alterations of the helical content of the residual helix of the constrained peptide result in a shift of the amide I′ band.[36] From the CD spectra of peptide **1** and peptide **2** and their unconstrained analogues at room temperature,[36] an increase of the helicity from approximately 40% to 80% is expected to occur in these peptides after disulfide bond splitting, if the equilibrium configuration can be adopted before thiyl radical recombination occurs. The concentration of unconstrained peptides at 2 ns can be estimated as above from the transient thiyl radical absorbance at 620 nm and the extinction coefficient of the *p*-aminophenylthiyl radical to be 0.03 mM. From the known changes in the IR spectrum[36] an absorbance *increase* near 1630 cm^{-1} on the order of 0.15 mOD is expected. A corresponding decrease is expected around 1650 cm^{-1}.

In contrast to this expectation, a net absorbance *decrease* of 0.15 mOD was observed at 1630 cm^{-1}. Furthermore, there is *no spectral shift*, the signal appears faster than 100 ps, and it decays in parallel with the thiyl radical recombination. These signals are not typical of α-helix formation. They strongly suggest that significant helix formation does not occur within 2 ns. This conclusion is consistent with recent results[62] obtained indirectly from the unfolding dynamics of short peptides after a temperature jump,[29] which indicates that helix formation occurs with a time constant of approximately 180 ns. In the present case the IR spectral changes are of course too small to detect at 50 ns because of the ever decreasing concentration of the ring-opened form of the peptide, as discussed in the Recombination Dynamics subsection.

Electric Field Effect on the Amide I′ IR Spectrum. As indicated earlier, we are proposing that the observed changes in the amide I′ region are caused by electric field effects from the changed charge distribution on the aminothiyl radicals after photolysis.

An electric field affects the frequencies as well as the intensities of IR transitions. Thus, contributions from both the vibrational Stark tuning rate ($\delta_{vE} = d\bar{\nu}/dE$) and the fractional change of the IR cross section ($\delta_{SE} = \sigma^{-1}\, d\sigma/dE$) can cause changes in the amide I′ IR region. Using various ab initio and semiempirical methods, several authors have calculated the vibrational Stark tuning rate and the fractional change in the infrared cross section for the C═O stretching vibration of CO[63−65] as well as in formaldehyde.[66,67] These calculations yielded values around 5×10^{-7} cm^{-1}/(V/cm) for $\delta_{\nu E}$ and -3×10^{-9}/(v/cm) for δ_{SE}, with the direction of the electric field directed from C to O. The predictions are in good agreement with experimental results for CO adsorbed on electrodes.[68,69] In the calculations described below additional fields in the range 10^8 V cm^{-1}, corresponding to the field at 4 Å from a unit charge, could be experienced by some of the amide carbonyls after photodissociation of the S−S bond. These tuning rates imply that this field could result in a shift of 50 cm^{-1} of a carbonyl stretching frequency and a fractional change of −0.3 in its intensity. A vibrational Stark effect, observed in the amide region of the reaction centers of photosynthetic bacteria following light-induced charge separation,[70] was consistent with these theoretical estimates.

We now summarize the data that point to the existence of an electric field effect. The observed bleaching signal of the IR absorbance at 1630 cm^{-1} in peptide **2** appeared in less than 100 ps and decayed in parallel with the thiyl radical recombination. These results indicate that the IR signal change correlates with the concentration of the ring-opened unconstrained peptide. The anisotropy measurements on the visible transients of the radicals have shown no evidence of significant internal peptide backbone motions within the first 100 ps. Therefore the observed transient IR signals, which appear in less than 100 ps, cannot be readily explained by such motions. We consider it more likely that a vibrational Stark effect is responsible for the changes in the IR spectrum. The origin of the electric field needed for the Stark effect is attributed to the changes in the sulfur and nitrogen partial charges that occur after disulfide bond dissociation. As discussed above, the charge separation occurs for the model aminophenylthiyl radicals and is therefore also expected to be present in peptide **2**. This interpretation obviously is consistent with the rapid formation of the IR transient and its disappearance paralleling the thiyl radical recombination. At a delay time of 100 ps, a bleach of approximately 0.4 mOD was observed. The concentration of unconstrained peptides at this time was estimated from the transient thiyl radical absorbance at 620 nm and the extinction coefficient of the p-aminophenylthiyl radical[50] to be about 0.06 mM, corresponding to a fraction of 5×10^{-3} of the overall peptide concentration. From the known sample absorbance at 1630 cm^{-1}, the IR transient can be estimated to correspond to a bleach of about 25% of the amide I′ band in these peptides. We now show that these observed signal magnitudes are consistent with theoretical estimates based on what is known about the structures of the peptides.

For a quantitative simulation of the vibrational Stark effect, we estimated the shift and intensity change for each carbonyl C═O stretch vibration after an electron is transferred from the nitrogens to the sulfur atoms. These simulations made use of the peptide **2** structures calculated by MD simulations.[36] The electric field component along the axis of each C═O bond was calculated after placing one negative elementary charge on the S atoms and one positive elementary charge on the amino group of the modified tyrosines. A homogeneous dielectric constant of 1 was assumed for the electric field calculation, thus neglecting any solvent screening effects.[71] All carbonyl vibrational transitions in the absence of the electric field were assumed to have a Gaussian shape, centered at 1640 cm^{-1} with a full width at half-maximum of 40 cm^{-1}, in accordance with the peptide ground-state infrared spectrum. The spectrum of each individual carbonyl vibration in the presence of the field was calculated using the numerical values for $\delta_{\nu E}$ and δ_{SE}, given earlier. As an example, the individual carbonyl spectra calculated for one particular structure are shown as dotted lines in Figure 7A. We find that only the carbonyls having optimum orientation and close proximity to at least one of the charges

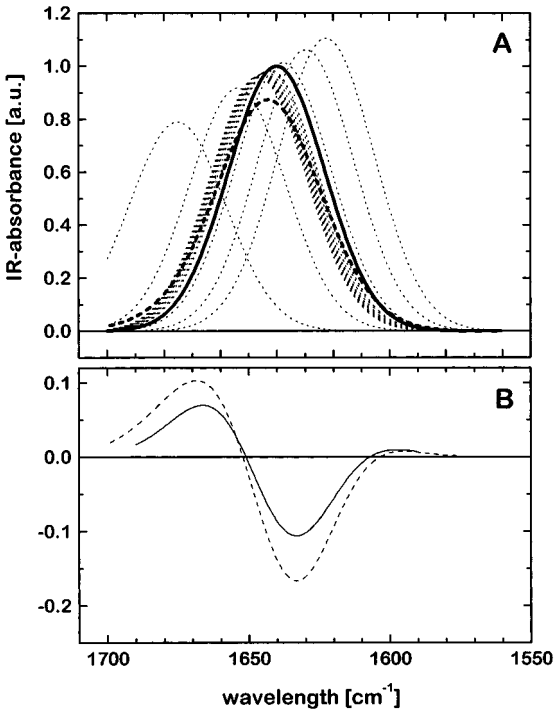

Figure 7. Simulated carbonyl IR spectra in peptide **2** after internal charge separation between the sulfur atoms and the amino group of the modified tyrosines. (A) Spectra calculated for one particular structure: carbonyl spectrum without electric field (solid line), spectra of the individual carbonyls after internal charge separation (dotted lines), and composite peptide spectrum after internal charge separation (dashed line). (B) Difference between the peptide spectrum before and after internal charge separation, calculated for the same structure as in A (dashed line) and averaged over a representative set of calculated spectra (solid line). See text for details.

show a significant Stark effect. For the particular peptide structure used in Figure 7A, only four carbonyls show a significant effect, with the largest shift being induced in one of the tyrosine carbonyls.

The overall peptide spectrum in the presence of the field, calculated by averaging the spectra of the individual carbonyls, is shown in Figure 7A. Since shifts to both higher and lower frequency are found for the individual carbonyls, the overall effect corresponds to a *broadening* of the amide I′ band. Figure 7B shows the difference between the simulated peptide spectra before and after internal charge separation, for the particular structure used in Figure 7A (dashed line) and averaged over a representative set of calculated structures (solid line). This difference spectrum should be compared directly with the experimental difference spectrum of Figure 4 after subtraction of the D_2O heating signal. A good agreement between the simulations and the experimental results is found. At the maximum frequency of the band, the simulations predict a reduction of the absorbance by 10% as a result of the electric field from the internal charge separation. This compares reasonably well with the 25% reduction observed at 1630 cm^{-1}, given the approximate nature of the simulations, the uncertainties with respect to structure, the amount of internal charge separation, and the values of $\delta_{\nu E}$ and δ_{SE} estimated from other systems.

It is concluded that the observed transient IR signals are consistent with a vibrational Stark effect due to charge redistribution at the modified tyrosines after disulfide bond splitting. The internal charge separation may also modify the vibrational transitions directly by shifting small amounts of charge through the σ bonds of the peptide backbone. This could yield an additional contribution to the observed IR signals, having a physically different origin from the *through-space* vibrational Stark effect considered above.

Prospects

The introduction of an aryl disulfide into a peptide sequence has resulted in the measurement of unprecedented kinetic processes in peptide conformaional dynamics. The recombination of the thiyl radicals is found to follow a power law behavior over 7 decades of time. We propose that conformational relaxation of the peptide is responsible for this unusual behavior. Following photolysis, recombination occurs readily because the radical centers are close spatially. As time progresses, the peptide begins to extend into a more helical ensemble, in which the radical centers are spaced further apart and recombination is slowed. To evaluate this hypothesis, we are investigating the effects of helix-favoring or helix-disrupting solvents on kinetics of recombination. Furthermore, a study of the kinetics of recombination of peptides of varying chain lengths and helix propensities should help define the conformational basis for the observed kinetics.

Acknowledgment. This work was supported by NIH grants GM12592 (to R.M.H.) and GM54616 (to W.F.D.) and by instrumentation developed through NIH-RR1308 (to R.M.H.). M.V. gratefully acknowledges the Deutsche Forschungsgemeinschaft for a research fellowship. We thank Jim Lear for stimulating discussions.

References and Notes

(1) Borisevich, N. A.; Lysak, N. A.; Melnichuk, S. V.; Tikhomirov, S. A.; Tolstorozhev, G. B. In *Ultrafast Phenomena in Spectroscopy*; Klose, E., Wilhelmi, B., Eds.; Springer-Verlag: Berlin, Heidelberg, 1990; Vol. 49, pp 276−281.

(2) Ernsting, N. P. In *Ultrafast Phenomena VIII*; Martin, J. L., Migus, A., Mourou, G. A., Zewail, A. H., Eds.; Springer-Verlag: Berlin, Heidelberg, 1993; p 638.

(3) Volk, M.; Kholodenko, Y.; Lu, H. S. M.; Degrado, W.; Gooding, E.; Hochstrasser, R. M. Femtosecond Dissociation and Geminate Recombination of Aromatic Disulfides in Solution, in course of publication.

(4) Phillips, C. M.; Mizutani, Y.; Hochstrasser, R. M. *Proc. Natl. Acad. Sci. U.S.A.* **1995**, *92*, 7292−7296.

(5) Dyer, R. B.; Williams, S.; Woodruff, W. H.; Gilmanshin, R.; Callender, R. H. *Biophys. J.* **1996**, *70*, A177.

(6) Wilemski, G.; Fixman, M. *J. Chem. Phys.* **1974**, *60*, 866.

(7) Szabo, A.; Sculten, K.; Schulten, Z. *J. Chem. Phys.* **1980**, *72*, 4350.

(8) Pastor, R. W.; Zwanzig, R.; Szabo, A. *J. Chem. Phys.* **1997**, *105*, 1878.

(9) Rouse, P. E. *J. Chem. Phys.* **1953**, *21*, 1272.

(10) Kim, P. S.; Baldwin, R. L. *Annu. Rev. Biochem.* **1990**, *59*, 631−660.

(11) Englander, S. W.; Mayne, L. *Rev. Biophys. Biomol. Struct.* **1992**, *21*, 243−265.

(12) Skolnick, J. S.; Kolinski, A.; Godzik, A. *Proc. Natl. Acad. Sci. U.S.A.* **1993**, *90*, 2099−2100.

(13) Eaton, W. A.; Thompson, P. A.; Chan, C. K.; Hagen, S. J.; Hofrichter, J. *Structure* **1996**, *4*, 1133−1139.

(14) Ptitsyn, O. B. *J. Protein Chem.* **1987**, *6*, 273−293.

(15) Karplus, M.; Weaver, D. L. *Nature* **1976**, *260*, 404−406.

(16) Dill, K. A. *Biochemistry* **1985**, *24*, 1501−1509.

(17) Dill, K. A.; Bromberg, S.; Yue, K.; Fiebig, K. M.; Yee, D. P.; Thomas, P. D.; Chan, H. S. *Protein Sci.* **1995**, *4*, 561−602.

(18) Sosnick, T. R.; Mayne, L.; Englander, S. W. *Proteins* **1996**, *24*, 427−432.

(19) Sosnick, T. R.; Jackson, S.; Wilk, R. R.; Englander, S. W.; DeGrado, W. F. *Proteins* **1996**, *24*, 427−432.

(20) Otzen, D. E.; Itzhaki, L. S.; F., E. N.; Jackson, S. E.; Fersht, A. R. *Proc. Natl. Acad. Sci. U.S.A.* **1994**, *91*, 10422−10425.

(21) Abkevich, V. I.; Gutin, A. M.; Shakhnovich, E. I. *Biochemistry* **1994**, *33*, 10026−10036.

(22) Guo, Z.; Thirumalai, D. *Biopolymers* **1995**, *36*, 83−102.

(23) Schwarz, G.; Seelig, J. *Biopolymers* **1968**, *6*, 1263−1277.

(24) Hammes, G. G.; Roberts, P. B. *J. Am. Chem. Soc.* **1969**, *91*, 1812−1816.

(25) Gruenewald, B.; Nicola, C. U.; Lustig, A.; Schwarz, G.; Klump, H. *Biophys. Chem.* **1979**, *9*, 137−147.

(26) Jones, C. M.; Henry, E. R.; Hu, Y.; Chan, C. K.; Luck, S. D.; Bhuyan, A.; Roder, H.; Hofrichter, J.; Eaton, W. A. *Proc. Natl. Acad. Sci. U.S.A.* **1993**, *90*, 11860−11864.
(27) Pascher, T.; Chesick, J. P.; Winkler, J. R.; Gray, H. B. *Science* **1996**, *271*, 1558−1560.
(28) Ballew, R. M.; Sabelko, J.; Gruebele, M. *Proc. Natl. Acad. Sci. U.S.A.* **1996**, *93*, 5759−5764.
(29) Williams, S.; Causgrove, T. P.; Gilmanshin, R.; Fang, K. S.; Callender, R. H.; Woodruff, W. H.; Dyer, R. B. *Biochemistry* **1996**, *35*, 691−697.
(30) Brooks, C. L. *J. Phys. Chem.* **1996**, *100*, 2546−2549.
(31) Tirado-Rives, J.; Jorgensen, W. L. *Biochemistry* **1991**, *30*, 3864−3871.
(32) Soman, K. V.; Karimi, A.; Case, D. A. *Biopolymers* **1993**, *33*, 1567−1580.
(33) Caflisch, A.; Karplus, M. *J. Mol. Biol.* **1995**, *252*, 672.
(34) Phillips, M.; Sytnik, A.; Hochstrasser, R. M. *J. Mol. Spectrosc.* **1997**.
(35) Marqusee, S.; Robbins, V. H.; Baldwin, R. L. *Proc. Natl. Acad. Sci. U.S.A.* **1989**, *86*, 5286−5290.
(36) Lu, H. S. M.; Volk, M.; Kholodenko, Y.; Gooding, E.; Hochstrasser, R. M.; DeGrado, W. F. *J. Am. Chem. Soc.* **1997**, *119*, 7173−7180.
(37) Asaki, M. T.; Huang, C. P.; Garvey, D.; Zhou, J.; Kapteyn, H. C.; Murnane, M. M. *Opt. Lett.* **1993**, *18*, 977.
(38) Wynne, K.; Reid, G. D.; Hochstrasser, R. M. *Opt. Lett.* **1994**, *19*, 895−897.
(39) Wynne, K.; Haran, G.; Reid, G. D.; Moser, C. C.; Dutton, P. L.; Hochstrasser, R. M. *J. Phys. Chem.* **1996**, *100*, 5140−5148.
(40) Hansen, P. A.; Moore, J. N.; Hochstrasser, R. M. *Chem. Phys.* **1989**, *131*, 49−62.
(41) Papp, S.; Vanderkooi, J. M.; Owen, C. S.; Holtom, G. R.; Phillips, C. M. *Biophys. J.* **1990**, *58*, 177−186.
(42) Nikogosyan, D. N.; Oraevsky, A. A.; Rupasov, V. I. *Chem. Phys.* **1983**, *77*, 131−143.
(43) Wiesenfeld, J. M.; Ippen, E. P. *Chem. Phys. Lett.* **1980**, *73*, 47−50.
(44) Migus, A.; Gauduel, Y.; Martin, J. L.; Antonetti, A. *Phys. Rev. Lett.* **1987**, *58*, 1559−1562.
(45) Long, F. H.; Lu, H.; Eisenthal, K. B. *Chem. Phys. Lett.* **1989**, *160*, 464−468.
(46) Long, F. H.; Lu, H.; Eisenthal, K. B. *Phys. Rev. Lett.* **1990**, *64*, 1469−1472.
(47) Reuther, A.; Laubereau, A.; Nikogosyan, D. N. *J. Phys. Chem.* **1996**, *100*, 16794−16800.
(48) Lian, T. S.; Locke, R. B.; Kholodenko, Y.; Hochstrasser, R. M. *J. Phys. Chem.* **1995**, *98*, 11648.
(49) Morine, G. H.; Kuntz, R. R. *Chem. Phys. Lett.* **1979**, *67*, 552−554.
(50) Lembke, R. R.; Natarajan, L. V.; Kuntz, R. R. *J. Photochem.* **1983**, *21*, 814.
(51) The extinction coefficient of *p*-aminophenylthiyl radical was not determined in a water solvent. We used a value of 20 000 M^{-1} cm^{-1} for the extinction coefficient in water estimated by extrapolation from the measurements in other solvents (see ref 50).
(52) Scott, T. W.; Liu, S. N. *J. Phys. Chem.* **1989**, *93*, 1393−1396.
(53) The prime indicates deuterated amides.
(54) Krimm, S.; Bandekar, J. *Adv. Protein Chem.* **1986**, *38*, 181−364.
(55) At delay times of less than 100 ps a large transient absorbance of up to 10 mOD is observed in the infrared even in the absence of peptide. When irradiating a fresh area of the sample cell with 270 nm pulses, these signals initally are small but increase on the time scale of minutes in synchrony with the appearance of luminescent spots on the window. Therefore, we assign them to color centers induced in the CaF_2 windows by the pump pulses. Because of these large signals, it is impossible to measure the amide I′ response at delay times below 100 ps. At delay times larger than 100 ps these signals are smaller than 0.05 mOD, as is known from measurements on neat D_2O samples under identical conditions. Furthermore, they are wavelength independent in the region we have investigated and cancel when the data at 1605 and 1630 cm^{-1} are subtracted. No transient signals from these color-centers were observed when probing in the visible.
(56) DeGennes, P. G. *J. Phys. Lett.* **1985**, *46*, 639.
(57) Zimm, B. H.; Bragg, J. K. *J. Chem. Phys.* **1959**, *31*, 526−535.
(58) For a single component system $r = (2/5)\langle P_2(\cos\theta)\rangle$. When the pumped and probed transition dipoles are parallel $r = 0.4$ (corresponding to $\theta = 0$), and when they are perpendicular (corresponding to $\theta = \pi/2$) $r = -0.2$.
(59) The two aminotyrosines are not symmetry related in the constrained peptide structure. Thus the pump−probe anisotropy for the disulfide photodissociation is given by

$$r(t) = (2/5)\sum_k [\langle P_2[\cos\theta_{k1;1}]\rangle P_{k1;1} + \langle P_2[\cos\theta_{k2;1}]\rangle P_{k2;1}] \times \langle P_2[\cos\phi_1(t)]\rangle + \sum_k [\langle P_2[\cos\theta_{k2;2}]\rangle P_{k2;2} + \langle P_2[\cos\theta_{k1;2}]\rangle P_{kt;2}]\langle P_2[\cos\phi_2(t)]\rangle$$

where $\theta_{kn;m}$ is the angle between the dipole of the *k*th electronic transition of aminotyrosine *n* and the probed transition of the radical from aminotyrosine *m* (*n*, *m* = 1, 2). $P_{km;n}$ is the relative contribution to the signal from excitation of the *k*th transition of aminotyrosine *m* while probing the thiyl radical on end *n* of the peptide. There is as yet insufficient knowledge of the optical transitions of the aminotyrosine disulfide to evaluate $r(t)$ with confidence.
(60) Perrin, F. *J. Phys. Radium* **1934**, *5*, 497.
(61) Szabo, A. *J. Chem. Phys.* **1984**, *81*, 150.
(62) Using a two-state model for folding/unfolding and a measured equilibrium constant of 10 (favoring the folded conformation), it was concluded (see ref 29) that the folding rate of this peptide is $(16\ ns)^{-1}$. However, an error was made in this analysis: The relaxation time in a two-state model is given by the sum of the forward and backward rate; thus neither rate can be larger than $(160\ ns)^{-1}$. The correct value for the folding rate in this model, based on their published data, should be $(180\ ns)^{-1}$.
(63) Bauschlicher, C. W. *Chem. Phys. Lett.* **1985**, *118*, 307−310.
(64) Lambert, D. K. *J. Chem. Phys.* **1991**, *94*, 6237−6242.
(65) Bishop, D. M. *J. Chem. Phys.* **1993**, *98*, 3179−3184.
(66) Andres, J. L.; Duran, M.; A., L.; Bertran, J. *Chem. Phys.* **1991**, *151*, 37−43.
(67) Marti, J.; Lledos, A.; Bertran, J.; Duran, M. *J. Comput. Chem.* **1992**, *13*, 821−829.
(68) Kunimatsu, K. *J. Phys. Chem.* **1984**, *88*, 2195−2200.
(69) Lambert, D. K. *J. Chem. Phys.* **1988**, *89*, 3847−3860.
(70) Maiti, S.; Walker, G. C.; Cowen, B. R.; Pippenger, R.; Moser, C. C.; Dutton, P. L.; Hochstrasser, R. M. *Proc. Natl. Acad. Sci. U.S.A.* **1994**, *91*, 10360−10364.
(71) A justification for this assumption is that only those carbonyl vibrations that are in close vicinity of the charged groups significantly contribute to the overall effect, since the electric field decreases more rapidly than $1/(\text{distance})^2$ between the charges and the CO groups.